CONVERSION OF ELECTRON-BEAM ENERGY TO THERMAL RADIATION IN THIN FILMS

G. S. Romanov and M. V. Suzdenkov

UDC 536.423.1

Studies have been made on the conversion of electron-beam energy to radiation in a gold foil.

1. There are fairly numerous studies [1, 2] on the effects of high-current electron beams on metal targets. Particular interest attaches to measurements on thin heavy-metal foils (gold and platinum). In [3, 4] it was found that the absorption was much greater than the classical theory implies (anomalous effect). The similar effect for foils with low z is explained [5] from collective effects due to beam-plasma instability and turbulence resulting from the reverse current. The beam is absorbed in a thin corona layer and does not penetrate deep into the target. The measurements were made with polyethylene films and with tantalum and nickel foils.

With heavy-element foils, currents above the Alfvén current I_A produce anomalous deposition because the intrinsic magnetic field from the current magnetizes the beam electrons, whose Larmor radius becomes less than the characteristic beam size [2, 6]. The electric field does not penetrate the plasma because of the fairly high conductivity, whereas the magnetic field does penetrate, since the diffusion scale during the pulse length τ_0 = 100 nsec is comparable with the plasma-layer thickness. It has been shown [2] that the losses in a transcritical beam can be increased by a factor I/I_A by comparison with the one-particle loss model, and the effective penetration depth is reduced. For example, a rigorous calculation for a Bennett radial current profile shows that collective effects associated with the intrinsic magnetic field and the electrical parameters produce an anomaly factor $k = 1.5I/I_A$. This coefficient may be introduced into Bethe's formula [7] for the electron energy loss per unit mass path $x = \rho\ell$ to get the deposition in the foil as

$$\Phi(E) = \left|\frac{dE}{dt}\right| = K2\pi r_0^2 \frac{N_a z}{A} m_0c^2 \left[\frac{\varepsilon+2}{2}\ln\left(m_0c^2(\varepsilon+2)/I_0^2\right) + f^-(\varepsilon) - \delta\right] + \left|\frac{dE}{dx}\right|_r. \quad (1)$$

In (1), $\left|\frac{dE}{dx}\right|_r$ is the loss due to bremsstrahlung [7], δ the atomic-polarization correction, $f^-(\varepsilon)$ the electron energy function [7], E electron energy, and $\varepsilon = E/(m_0c^2)$, with

$$K = \begin{cases} 1.5\,I/I_A, & \text{if } I > 2/3\,I_A, \\ 1, & \text{if } I < 2/3\,I_A. \end{cases}$$

A beam carrying a current I for a time Δt and traveling along the oz axis from the start of the region ℓ_1 occupied by the material to the end ℓ_2 deposits energy

$$\Delta E = \int_{l_1}^{l_2} I/e\,\Delta t\,\Phi(E)\,\rho(l)\,dl. \quad (2)$$

As the foil thickness is usually much less than the penetration depth, one can neglect the angular spread in the beam electrons.

We simulate the effects on the foil in a two-dimensional approximation in a formulation close to that of [8, 9]. We assume that the beam is incident along the oz axis in a cylindrical coordinate system, while the foil lies between the planes z = 0 and z = $-a$. The complete equation system is

Sevchenko Applied Physics Research Institute, Lenin Belorussian University, Minsk. Translated from Inzhenerno-Fizicheskii Zhurnal, Vol. 55, No. 5, pp. 810-816, November, 1988. Original article submitted March 31, 1987.

0022-0841/88/5505-1281$12.50

$$\frac{\partial \rho}{\partial t} + \operatorname{div}(\rho \mathbf{W}) = 0, \quad \frac{\partial \rho u}{\partial t} + \operatorname{div}(\rho u \mathbf{W}) + \frac{\partial P}{\partial z} = 0,$$
$$\frac{\partial \rho v}{\partial t} + \operatorname{div}(\rho v \mathbf{W}) + \frac{\partial P}{\partial r} = 0, \quad \frac{\partial \rho E}{\partial t} + \operatorname{div}(\rho E \mathbf{W}) + \operatorname{div}(P \mathbf{W}) + \operatorname{div} \mathbf{F} - Q\rho = 0, \tag{3}$$

in which Q_ρ is the energy deposition defined by (1) and (2).

We integrated (3) numerically in several stages on an Euler net contining 4000 cells. In the first stage, we calculated the deposition from (1) and (2). In the second, we calculated the radiative loss from the vapor jet via a method that incorporated the radiation spectrum in the three-group approximation, with the absorption coefficients in each group independent of frequency and equal to the Planck averages for the spectral coefficients given as tables [10, 11]. In the third stage, we integrated the hydrodynamic equations by the large-particle method as extended to a nonadiabatic flow [12, 13].

The emission is described by the div **F** term in (3); a finite-difference expression for this term is obtained on the Euler net by solving the radiation transport equation along a ray in a certain direction [14]:

$$I_\nu(\tau) = \int_{\tau_0}^{\tau} \varkappa_\nu I_{\nu_e} \exp\left(-\int_{\tau'}^{\tau} \varkappa_\nu d\tau''\right) d\tau' + I_{0\nu} \exp\left(-\int_{\tau''}^{\tau} \varkappa_\nu d\tau'\right),$$
$$I_{\nu_e} = 2h\nu^3 c^{-1} [\exp(h\nu/kT) - 1]^{-1}. \tag{4}$$

The equilibrium one-sided integral flux is

$$B_e = \int_0^\infty B_{\nu_e} d\nu = \pi \int_0^\infty I_{\nu_e} d\nu = \sigma T^4.$$

The subscript ν indicates that the parameters are dependent on the quantum energy.

The angular distribution is incorporated in the two-flux approximation, with one-way fluxes in the positive direction + and negative direction − along the coordinate axes. It was assumed that the fluxes in spectral range n at each boundary of an Euler cell were normal to the side surfaces and were as follows for the boundaries along the oz axis (subscript i) and the oR axis (subscript j):

$$F^n_{i\pm\frac{1}{2},\,j} = F^{n+}_{i\pm\frac{1}{2},\,j} - F^{n-}_{i\pm\frac{1}{2},\,j}, \quad F^n_{i,\,j\pm\frac{1}{2}} = F^{n+}_{i,\,j\pm\frac{1}{2}} - F^{n-}_{i,\,j\pm\frac{1}{2}}, \tag{5}$$

in which n is the number of the spectral group and (i, j) is the Euler cell number.

We integrate (4) over the spectrum and multiply by π to get the radiation energy balance for each Euler cell for one-way fluxes along the oz and oR axes:

$$F^{n+}_{i+\frac{1}{2},\,j} = q^n_{i,\,j} + F^{n+}_{i-\frac{1}{2},\,j} \exp(-l^n_{i,\,j}),$$
$$F^{n-}_{i-\frac{1}{2},\,j} = q^n_{i,\,j} + F^{n-}_{i+\frac{1}{2},\,j} \exp(-l^n_{i,\,j}), \tag{6}$$

$$S_{j+\frac{1}{2}} F^{n+}_{i,\,j+\frac{1}{2}} = S_{j+\frac{1}{2}} q^n_{i,\,j} + S_{j-\frac{1}{2}} F^{n+}_{i,\,j-\frac{1}{2}} \exp(-\bar{l}^n_{i,\,j}),$$
$$S_{j-\frac{1}{2}} F^{n-}_{i,\,j-\frac{1}{2}} = S_{j-\frac{1}{2}} q^n_{i,\,j} + S_{j+\frac{1}{2}} F^{n-}_{i,\,j+\frac{1}{2}} \exp(-\bar{l}^n_{i,\,j}), \tag{7}$$

where the intrinsic-radiation flux is

$$q^n_{i,\,j} = \begin{cases} l^n_{i,\,j}\ B_{i,j}, & l^n_{i,\,j} < 1, \\ B^n_{i,\,j}, & l^n_{i,\,j} > 1. \end{cases} \tag{8}$$

In (6)-(8), $l^n_i = l^n_{i,\,j} = \varkappa^n_{ij} \Delta z_i$, $\bar{l}^n_{i,\,j} = \varkappa^n_{i,\,j} \Delta r_j = l^n_j$ are the optical thicknesses of the Euler cell along the coordinate axes, while $S_{j\pm\frac{1}{2}} = 2\pi r_{j\pm\frac{1}{2}} \Delta r$ are the areas of the side surfaces.

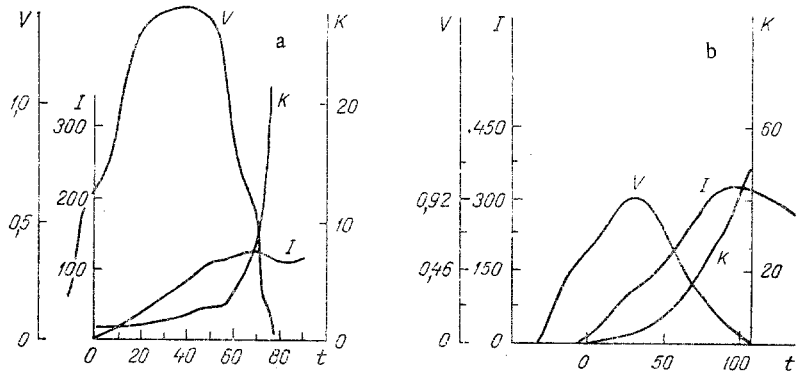

Fig. 1. Voltage and current waveform: a) measurements [3]; b) measurements [4]; V in MV, t in nsec, and I in kA.

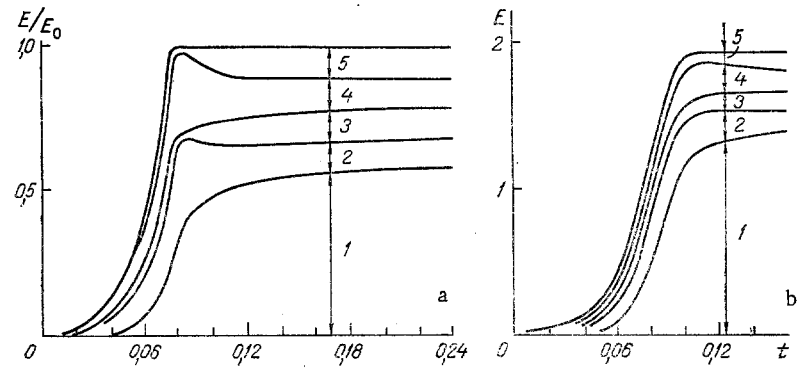

Fig. 2. Energy-distribution behavior on interaction: 1) energy emitted from region; 2) thermal component of energy in plasma ahead of foil; 3) kinetic component of energy in plasma ahead of foil; 4) thermal component of energy in plasma behind foil; 5) kinetic component of energy in plasma behind foil; a) calculation from [3] experiment; b) calculation from [4] experiment; E in kJ and t in μsec.

Equations (5) and (6) give a difference expression for the divergence in the integral radiation energy flux [10, 11]:

$$(\operatorname{div} F)_{i,j} = \frac{F_{i+\frac{1}{2},j} - F_{i-\frac{1}{2},j}}{\Delta z_i} + \frac{r_{j+\frac{1}{2}} F_{i,j+\frac{1}{2}} - r_{j-\frac{1}{2}} F_{i,j-\frac{1}{2}}}{r_j \Delta r_j} =$$

$$= \frac{2q_{i,j}}{\Delta z_i} - \frac{F^-_{i+\frac{1}{2},j} + F^+_{i-\frac{1}{2},j}}{\Delta z_i}(1 - \exp(-l_i)) + \frac{r_{j+\frac{1}{2}} + r_{j+\frac{1}{2}}}{r_j \Delta r_j} q_{i,j} -$$

$$- \frac{r_{j+\frac{1}{2}} F^-_{i,j+\frac{1}{2}} + r_{j-\frac{1}{2}} F^+_{i,j-\frac{1}{2}}}{r_j \Delta r_j}(1 - \exp(-\bar{l}_j)).$$

The fluxes were set to zero at the boundary of the working region at t = 0, while there was no intrinsic radiation. Equation (3) was closed from the tabulated equation of state for gold derived from Saha's model [15] with allowance for high degrees of ionization. The plasma absorption coefficients were derived by the method of [16].

2. Figure 1 shows current and voltage waveforms used as input in the calculations, together with the time dependence of the calculated anomaly factors K. The pulse lengths (Fig. 1) were 75 and 110 nsec, while the deposition radius was 0.1 cm. The gold foil thickness in the measurements (Fig. 1a) was 5 μm, or 10 μm in the experiment represented in Fig. 1b. The beam energy in the first waveform was 5.56 kJ, or 4.315 kJ in the second [3, 4].

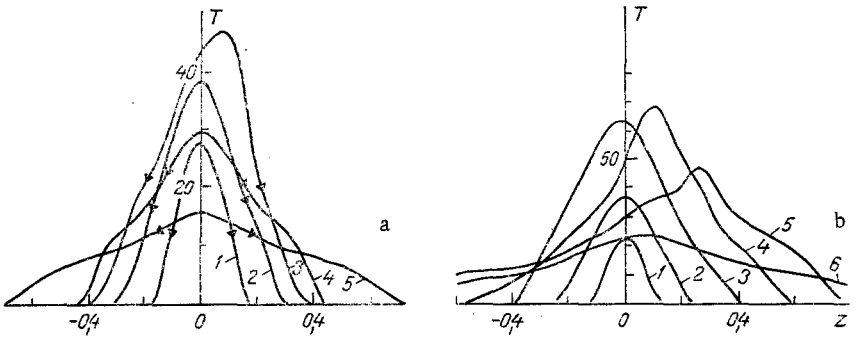

Fig. 3. Plasma temperature distribution along the oz axis: a) calculation from [3] experiments: 1) 49; 2) 66; 3) 75; 4) 82; 5) 115 nsec; b) calculation from [4] experiments: 1) 33; 2) 49; 3) 66; 4) 83; 5) 110; 6) 131 nsec.

The beam heats the foil, which evaporates, and the vapor is ionized. The highly ionized plasma expands parallel and antiparallel to the beam, while radiating rapidly. Figure 2 shows the absorbed energy distribution by components. In the first case, 0.245 kJ is absorbed (4.4% of the beam energy), with 58% of it lost from the plasma as radiation in the hard ultraviolet range, photon energy over 10 eV (third spectral group), which constitutes 2.5% of the beam energy (Fig. 2a). In the second, the anomaly is much larger, as is evident from K(t) in Fig. 1b. Here 45.5% of the beam energy is absorbed, and 71.3% of it constitutes radiation loss from the vapor jet. In the second experiment, 32.4% of the beam energy is converted to radiation in the hard ultraviolet range.

The absorption anomaly is more pronounced in the second case, since Fig. 3 shows the temperature distribution along the symmetry axis (initially, the foil is at z = 0). Although the visible plasma temperature is about 20 eV (the corresponding points relating to the boundary of the opaque region are shown in Fig. 3), the temperature at the center of the foil attains 50-70 eV. In the second case, the peak temperature attains 70 eV and was displaced in the opposite sense to the beam by 0.1 cm, and at the end of the pulse it attained 50 eV and was displaced by 0.3 cm. This shows that the beam energy is extensively absorbed at the leading edge of the plasma and does not at that time attain the rear region. That effect was less pronounced in the first case, although at the end of the t = 40 nsec pulse, the foil material had become opaque to the beam. Although there is some asymmetry in the temperature patterns on the two sides of the foil, there was no appreciable asymmetry in the vapor expansion dynamics.

Figure 4 indicates the emission power and spectrum, which are important in diagnosis. At the end of the pulse, in both cases there is a sharp burst, power up to 4×10^3 MW. The main radiative losses lie in the hard UV range above 10 eV, while the power levels in the first and second groups are less by two orders of magnitude, being at most 20 MW. In both cases, the emission power perpendicular to the beam (lateral direction) is greater than that along the beam (from the foil) because of preferential absorption on the incident side.

These calculations agree well with measurements [1-4]. Estimates of the peak radiated power in [3] (Fig. 1a) are $2\text{-}3 \times 10^9$ W in the diode gap and $0.6\text{-}1.2 \times 10^9$ W from the outer side of the foil, with relatively little deposition in the foil plasma (about 10% of the beam energy). The radiated power levels in these directions are calculated as 4×10^9 and 1×10^9 W correspondingly. There is in both cases a correspondence between the peak emission signal and the peak on the energy deposition curve [3]. The main deposition and the maximum emission occur when the voltage on the diode is falling.

Any increase in current (Fig. 1b) causes stronger absorption in the plasma. When the beam electrons are highly magnetized, the anode foil plasma may [2, 4] absorb up to half the beam energy, when the temperature is estimated as 30-40 eV.

The model thus describes the basic trends well and can be used to interpret experiments.

NOTATION

r_0, classical electron radius; N_a, Avogadro's number; I_0, mean ionization potential; e, electron charge, u and v, axial and radial components of the velocity vector W; ρ, den-

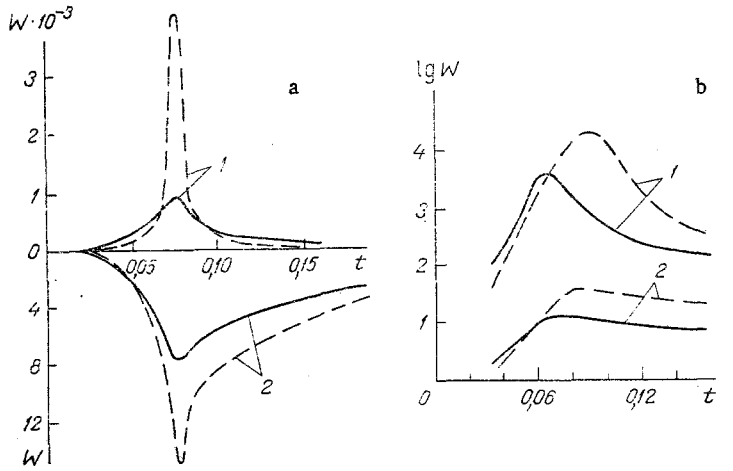

Fig. 4. Behavior of radiation power from foil: 1) total power; 2) power in spectral range below 10 eV; solid line along beam propagation direction; dashed line perpendicular to beam axis; a) [3] experiments; b) [4] experiments; log W and W in MW and t in μsec.

sity; P, pressure; E, total specific energy; F, radiation flux energy integrated over the spectrum; Q, specific energy deposition rate; I_ν, spectral intensity; $\varkappa_\nu$, spectral absorption coefficient corrected for induced emission.

LITERATURE CITED

1. M. V. Babykin, Surveys of Science and Engineering, Plasma Physics [in Russian], Moscow (1980), Vol. 1, Part 2, pp. 5-80.
2. L. I. Rudakov, Fiz. Plazmy, 4, No. 1, 72-77 (1978).
3. M. V. Babykin, K. A. Baigarin, A. V. Bartov, et al., Pis'ma Zh. Éksp. Theor. Fiz., 30, No. 7, 435-438 (1979).
4. M. W. Babykin, K. A. Baigarin, A. V. Bartov, et al., Third Internat. Topical Conf. on High Electron and Ion Beam Research and Technology, Novosibirsk, 3-6 July (1979). Book of Abstracts, p. 56.
5. K. Imasaki, S. Miyamoto, et al., Phys. Rev. Lett., 43, No. 26, 1937-1940 (1979).
6. Yu. M. Gorbulin, V. V. Gorev, S. F. Grigor'ev, et al., The Interactions of a High-Current Relativistic Electron Beam with Matter [in Russian], Preprint IPM AN SSSR im. M. V. Keldysh, No. 113, Moscow (1984).
7. A. F. Akkerman, Yu. M. Nikitushev, and V. A. Botvin, Monte Carlo Calculations on Fast Electron Transport in Matter [in Russian], Alma Ata (1972).
8. G. S. Romanov and M. V. Suzdenkov, Dokl. Akad. Nauk BSSR, 26, No. 6, 496-499 (1982).
9. G. S. Romanov, M. V. Suzdenkov, A. V. Teterev, and G. A. Fokov, Inzh.- Fiz. Zh., 57, No. 6, 952-957 (1984).
10. M. A. El'yashevich, G. S. Romanov, and Yu. A. Stankevich, Proceedings of the Fourth All-Union Conference on Radiating-Gas Dynamics [in Russian], Vol. 1, Moscow (1981), pp. 90-101.
11. G. S. Romanov and V. V. Urban, Proceedings of the Fourth All-Union Conference on Radiating-Gas Dynamics [in Russian], Vol. 1, Moscow (1981), pp. 12-20.
12. O. M. Belotserkovskii and Yu. M. Davydov, Zh. Vychisl. Mat. Mat. Fiz., 11, No. 1, 182-207 (1971).
13. G. S. Romanov, M. V. Suzdenkov, and A. V. Teterev, Zh. Vychisl. Mat. Mat. Fiz., 21, No. 3, 798-803 (1981).
14. Ya. B. Zel'dovich and Yu. P. Raizer, The Physics of Shock Waves and High-Temperature Hydrodynamic Phenomena [in Russian], Moscow (1963).
15. S. I. Kas'kova, G. S. Romanov, and K. L. Stepanov, Ionic Composition and Thermodynamic Functions for an Aluminum Plasma [in Russian], Dep. No. 612, BelNIINTI (1983).
16. G. S. Romanov, L. K. Stanchits, and K. L. Stepanov, Tables of Mean Group Absorption Coefficients for Aluminum Plasmas [in Russian], Dep No. 837, BelNIINTI (1984).